Optical and ultrasonic signatures of femtosecond pulse filamentation in fused silica

Vygantas Mizeikis,[1,a)] Saulius Juodkazis,[2] Tadas Balčiūnas,[2,b)] Hiroaki Misawa,[2] Sergey I. Kudryashov,[3] Vladimir D. Zvorykin,[3] and Andrei A. Ionin[3]
[1]*Division of Global Research Leaders, Research Institute of Electronics, Shizuoka University, 3-5-1 Johoku, Naka-ku, Hamamatsu 432-8561, Japan*
[2]*Research Institute for Electronic Science, Hokkaido University, Sapporo 001-0021, Japan*
[3]*P.N. Lebedev Physical Institute, Russian Academy of Sciences, 119991 Moscow, Russia*

(Received 4 March 2009; accepted 8 May 2009; published online 19 June 2009)

Millimeter-long filaments and accompanying luminous plasma and defect channels created in fused silica by single, moderately focused femtosecond laser pulses with supercritical powers were probed *in situ* using optical imaging and contact ultrasonic techniques. Above the threshold pulse energy $E_{opt}=5\ \mu J$ corresponding to a few megawatt power, the pulses collapse due to self-focusing and the nonlinear focus moves upstream with increasing pulse energy. Behind the focus, elongated, gradually narrowing awl-shaped channels of electron-hole plasma and luminescent defects are produced. In the channels, whose dimensions generally depend on the pulse energy, supercontinuum emission propagating downstream the channels occurs, although its observation requires elevated pulse energies above 25 μJ in order to compensate energy dissipation in the channels. Ultrasonic side-view imaging of the channels, conducted from a few millimeters distance, reveals predominantly compressive pressure transients. The compressive signals are observed above the same threshold pulse energy E_{opt}, and their amplitude increases linearly with the laser pulse energy, simultaneously exhibiting significant temporal broadening of the corresponding pulsewidths, reflecting square root dependence of the channel length and sublinear ($\propto E^{3/4}$) dependence of the source pressure on the pulse energy. Altogether, these optical and ultrasonic studies demonstrate filamentary pulse propagation with considerable dissipation ($\sim 10\ cm^{-1}$) in the awl-shaped subcritical plasma channels rich with generated point defects and optical damage sites.
 [DOI: 10.1063/1.3148249]

I. INTRODUCTION

Filamentation of femtosecond laser pulses in bulk dielectrics involves propagation of micrometer-sized light bullets over distances much longer than their diffraction length without any external guiding, and simultaneous generation of long electron-hole plasma (EHP) channels with micrometric cross sections, which are recognizable from transient luminescence and/or permanent photomodification of the host dielectric via point defect generation or optical ablation.[1,2] Due to small spatiotemporal envelope of the filaments, their detailed probing is a challenging experimental task. Although both dynamic monitoring of nonlinear spatiotemporal transformations of femtosecond pulses (such as harmonics and supercontinuum (SC) generation as well as pulse broadening effects) and postirradiation monitoring of longer-lived features (such as plasma channels, defect luminescence, or permanent damage tracks) have been reported so far, overcoming of experimental difficulties typically leads to significant loss of information on EHP dynamics, one of the key characteristics of filaments in photoexcited dielectrics.[1–5] Moreover, accurate spatially and temporally resolved measurements of crucial parameters of filaments, such as deposited optical energy and photogenerated carrier density in subcritical, optically opaque plasmas[1–5] have not been available yet, thus limiting the possibilities to develop adequate theoretical modeling of the filamentation in solids.[1,2]

At the same time it is well known that dense plasmas generate intense ultrasonic waves carrying important information about various parameters of the plasmas.[6–8] Ultrasonic effects may also provide important insights into structural modification of solid dielectrics during their microscale optical breakdown, where they are known to be involved in creation of local mass density variations,[9–11] or in formation of amorphous phases of natively crystalline materials.[12] Recently, ultrasonic probing has proven to be a simple and highly sensitive technique for remote monitoring of the fine axial structure of femtosecond laser filaments in air via spatially resolved relative measurements on the subsequent low-density plasmas.[13] Also, threshold energy and ultrasonic amplitudes were measured earlier for microscale optical breakdown in water.[14] Femtosecond filamentation in bulk solid dielectrics has received less attention so far. Although earlier we have reported some results on filamentation in bulk silica glass and fused silica,[15,16] comprehensive ultrasonic studies of filamentation and related phenomena—ionization, defect formation, and ablation—in bulk dielectrics, which would reveal their fundamental features, have not yet been performed.

[a)]Electronic mail: dvmzks@ipc.shizuoka.ac.jp.
[b)]Permanent address: Laser Research Center, Department of Quantum Electronics, Vilnius University, Saulėtekio 9, LT-2040 Vilnius, Lithuania, and Altechna Co., Ltd., Konstitucijos 23C-604, LT-08105 Vilnius, Lithuania.

In this work we report on spatially resolved *in situ* optical and ultrasonic imaging of self-focusing and filamentation of single femtosecond laser pulses with supercritical pulse powers in fused silica. The experiments reveal formation of millimeter-long, gradually narrowing channels filled by EHP and luminescent defects. The channels originate in the nonlinear focus above the single-shot threshold energy of 5 μJ due to self-focusing of the incident laser pulses with megawatt powers, and extend upstream with increasing pulse energy, demonstrating an awl-shaped damped filamentary structure. At incident pulse energies larger than 25 μJ, the energy dissipation in the channels is overcompensated and white-light SC is observed in the far field beyond the channels. Amplitudes of the recorded ultrasonic transients, signifying predominantly compressive phases, become observable above the same threshold pulse energy of 5 μJ, and increase linearly with pulse energy. Simultaneously, temporal broadening of the transients due to elongation of ultrasonic source within the channel is observed, reflecting the square root energy dependence of the channel length and retrieving the sublinear ($\propto E^{3/4}$) source pressure dependence on the pulse energy. This indicates that ultrasonic signals originate from warm subcritical plasmas within the awl-shaped filamentary channels, which subsequently produce isomorphic damage to the material via point defect generation.

II. SAMPLES AND EXPERIMENTAL SETUP

The samples used for these studies were blocks of fused silica (FS) glass (Seiken, Inc.) with refractive index $n_0 \approx 1.5$ at the wavelengths of 800 and 1030 nm (Ref. 17) used in our experiments (see below). To facilitate single-shot exposure conditions, the sample was mounted on a three-axis mechanical translation stage, which was smoothly translated in the plane perpendicular to the pulse propagation direction. Velocity of translation was sufficiently large to ensure that each pulse was incident on fresh, previously unexposed regions of the sample.

Two femtosecond lasers were used as irradiation sources. The first one was a Hurricane Ti:Sapphire amplified laser system (Spectra Physics) producing pulses of $\tau_p \approx 150$ fs duration full width at half maximum (FWHM) at an adjustable rate of up to $f=1$ kHz and a central wavelength $\lambda_c=800$ nm. The second source was a Yb:KGW laser system Pharos (Light Conversion, Ltd.) delivering pulses with parameters $\tau_p \approx 300$ fs (FWHM), $\lambda_c=1030$ nm, and maximum repetition rate $f=200$ kHz.

Combined ultrasonic and optical imaging experiments in FS were conducted using the 800 nm laser system. Optical radiation was coupled into the sample by focusing the pulses with a glass lens having focal distance $F=100$ mm. For the laser beam diameter of 7 mm the resulting effective numerical aperture is NA=0.035. The latter value allows one estimate lateral radius of the Gaussian beam waist at $1/e^2$ intensity level as $w_0=\lambda[n_0^2-\mathrm{NA}^2]^{1/2}/\pi\mathrm{NA} \approx 12$ μm and Rayleigh length $l_0=\lambda(n_0^2-\mathrm{NA}^2)/\pi\mathrm{NA}^2 \approx 0.5$ mm. For visualization of the optical damage to the sample, FS was additionally irradiated by 1030 nm pulses of the second laser system using a tighter focusing objective lens with numerical aperture NA=0.32. The side view of transient luminous channels resulting from EHP and defect luminescence were imaged *in situ* using a charge-coupled device (CCD) camera. Postirradiation imaging of optical damage tracks was performed using an optical microscope equipped with an objective lens with NA=0.9 and magnification factor 100×.

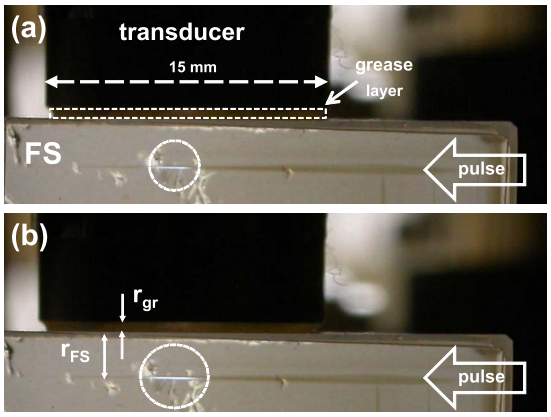

FIG. 1. (Color online) Geometry of ultrasonic imaging experiments and side-view images of plasma channels at laser pulse energies of $E=20$ (a) and 40 μJ (b). Cylindrical enclosure of the ultrasonic transducer is seen as a dark, 15 mm wide rectangle mounted to slide on the top surface of the FS sample. The layer of vacuum grease of thickness r_{gr} between the transducer and the sample is outlined by the rectangle in (a). Side face of the FS sample is seen as the brighter and wider, horizontally oriented area at the bottom of the images. The laser beam enters FS sample through the right side wall as indicated by the arrows. The plasma channels are emphasized by the dashed circles. Dark channels in front and behind the plasma channels represent integrated contribution of damage traces left by preceding pulses (in the same horizontal plane but at different lateral positions).

The geometry of ultrasonic imaging experiments is explained in Fig. 1. The ultrasonic response was recorded using MiniWAT-2 transducer (UC VINFIN) with sensitive area of (8×8) mm^2 and an electronic preamplifier. The combined bandwidth of the transducer and preamplifier was $\Delta f \approx 30$ MHz, and sensitivity of about 10 V/atm was achieved. The transducer was mounted to slide on the flat top surface of the sample, which was covered by a lubricating 0.3 mm thick layer of vacuum grease. The laser beam entered the sample through the polished side wall with its waist formed a few millimeters below the center of the transducer. During the experiments, constant relative positions of the laser beam and the transducer were maintained, while the sample was translated laterally as mentioned above. Voltage transients from the transducer, representing ultrasonic response of the material excited by single laser shots, were recorded using 50 Ω input of Tektronix TDS-5104 digital storage oscilloscope. The oscilloscope was triggered externally via another 50 Ω input channel using a fast photodiode with 175 ps rise time (Alphalas, Gmbh), which was fed by a weak laser pulse split from the irradiating pulse.

It is instructive to note that far-field ultrasonic imaging provides information about relative variations of ultrasonic pressure parameters rather than their absolute values in the ultrasonic source due to the following circumstances. While ultrasonic transients, as-generated by the source, have bandwidth extending to gigahertz frequencies,[18–20] real transients measured by detectors in the ultrasonic far-field are always

modified by dissipation effects in the FS and the grease layer, which distort and damp the waveforms via frequency-dependent dissipation, leading to their broadening and decrease in their amplitudes. The damping coefficient of FS is much lower, than that of the grease, but the initial pressure transients in the silica sample are much steeper (subnanosecond widths), resulting in much stronger damping of their high-frequency components.[20–23] Finally, geometric factors such as relative positions and effective sizes of the ultrasonic source and the transducer are important for diffraction effects.[24] In this particular ultrasonic far-field study we have paid attention to variations of the ultrasonic pulse amplitude, width, and waveform shape with the laser pulse energy in order to retrieve details such as EHP density and its spatiotemporal dynamics.

III. EXPERIMENTAL RESULTS

A. Optical imaging

Preliminary insight into phenomenological aspects of femtosecond supercritical pulse propagation in FS can be gained from optical imaging of bright, bluish channels, appearing and extending in the sample over several millimeters as shown in Fig. 1. The emission comes from EHP and/or luminescent defects exhibiting in FS the strongest spectral peak at 280 nm, medium intensity peaks near 400 and 470 nm, and weak peaks near 550 and 630 nm wavelengths.[25–28] In our experiments the channels first become visible on the CCD camera as pointlike bluish "sparks" at pulse energies above the threshold value $E_{opt}=5\pm1$ μJ. The spark occurs at a distance of $\approx$60 mm from the $F=100$ mm focusing lens due to collapse of the beam via self-focusing, providing in accordance with Marburger's formula[1] extra vergence $\sim10-10^2$ D. The strong role of self-focusing can be expected, since above E_{opt} our laser pulses have peak powers in excess of 30 MW, while the critical self-focusing power in FS at the wavelength of 800 nm is $P_{crit}\approx2$ MW.[29] Assuming negligible pulse broadening (characteristic group velocity dispersion length L_{GVD} in FS for 150 fs pulses is about 3×10^2 mm), and taking the beam waist area estimated above for linear focusing, one can deduce that E_{opt} corresponds to the peak intensity $I_{opt}=E_{opt}/(\pi w_0^2)\tau_p \approx5$ TW/cm^2, which is well below the measured value of bulk optical breakdown/damage threshold in FS $\approx50-60$ TW/cm^2.[3,30,31]

Among other well-known attributes of self-focusing is the gradual "upstream" elongation of the visible channels (toward the excitation source) we observe with increasing pulse energy, which signifies upstream movement of the nonlinear focus.[7] The total channel length b is typically much larger than the linear focal Rayleigh length $l_0\approx0.5$ mm, as can be seen from Fig. 1, where $b\approx1.2$ and 1.8 mm for $E=20$ and 40 μJ, respectively, are observed. In addition, downstream-propagating conical SC emission was observed above the threshold $E_{SC}=25\pm3$ μJ in the far field after the FS sample, which is also a signature of self-focusing.[1,2,32,33] The fairly high value of E_{SC} may result from considerable attenuation of both the fundamental and converted radiation in the material, or in the transient EHP generated at the leading edge of the irradiating laser pulse.

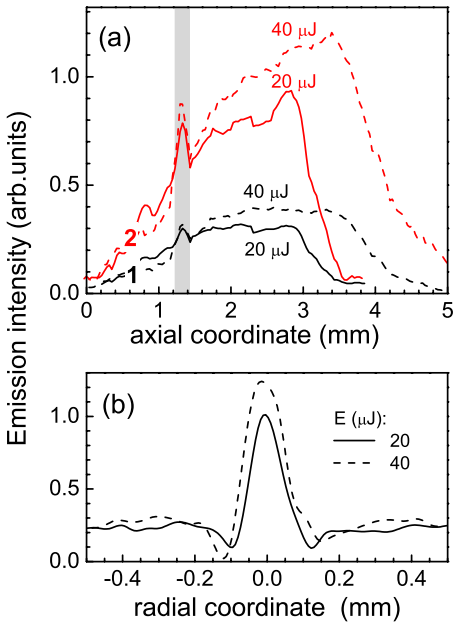

FIG. 2. (Color online) Intensity distribution within luminous channels vs axial (a) and radial (b) coordinates at different laser pulse energies of $E=20$ and 45 μJ. In (a) the axial profiles measured in the central part of the cross section of filaments and radially integrated profiles are labeled by "1" and "2," respectively. In (b), the radial profiles are taken at the axial coordinate of 2.3 mm. Laser pulse propagates from right to left, as in Fig. 1. The gray-shaded box marks the coordinate range containing a false peak due to a scratch on the sample surface.

Distribution of the emission intensity within the luminous channels in Fig. 1 qualitatively represents distribution of EHP and photogenerated point defects. Figure 2 shows emission profiles versus axial and radial coordinates, taken for the same pulse energies as in Fig. 1. Since laser pulse travels backward in Figs. 2(a) and 2(b), the filaments can be described as having a sharp leading edge and a slower two-part trailing edge. The first part (from approximately 3.5 down to 1.5 mm), where intensity variations are weak, has the length $b\approx1-2$ mm. Notice, that intensity of the channel core shown in Fig. 2(a) exhibits a plateau in this region (the region of filamentary propagation), with peak intensities of axial and radial profiles scaling as $E^{1/4}$, whereas the corresponding radially integrated profile slowly decreases. In the second part (at coordinates smaller than approximately 1.5 mm), the channel emission intensity quickly drops down, approaching exponential decrease in Fig. 2(a) (the region of damped laser beam propagation). While the presence of sharp leading edge makes the upstream shift of filaments with pulse energy clearly visible, the pseudoexponential trailing edge is consistent with the awl-shaped cross-sectional side views of the channel in Fig. 1 (further illustration is also given in Fig. 3 below) and the assumption about considerable dissipation of the laser pulse energy in the channels. According to Fig. 2(a), an effective length of ~10 cm^{-1} can be ascribed to the dissipation.

As can be seen from Fig. 2(b), shape of radial intensity profiles in the intensity plateau (filament) region is nearly

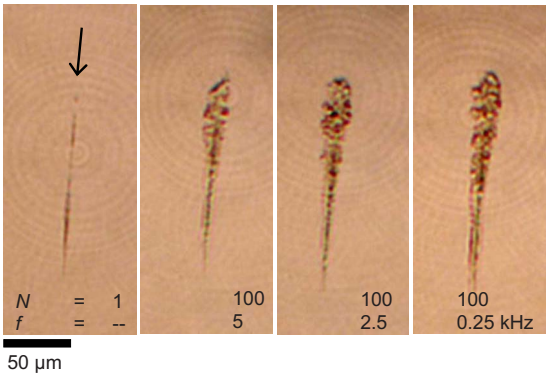

FIG. 3. (Color online) Side-view optical images of damage traces of filaments in bulk FS after irradiation by N pulses of 300 fs duration, 60 μJ energy, and central wavelength of 1030 nm. The pulses were focused by a lens with NA=0.32; their propagation direction is indicated by the arrow.

independent of the laser pulse energy. The diameter of filaments, $a_{\mathrm{fil}} \sim 100$ μm, determined from the optical images, is somewhat larger than the known values of $a_{\mathrm{fil}} \sim 10$ μm characteristic for solid dielectrics.[1,5] However, it is very likely that our imaging of the filaments by the CCD camera without any external magnifier does not have the resolution needed for resolving the radial intensity profiles. With this assumption, and using the literature value of a_{fil}, local intensity in the nonlinear focus can be estimated as $I_{\mathrm{opt}}^{\mathrm{NL}} = E_{\mathrm{opt}}/a_{\mathrm{fil}}^2 \tau_p \approx 30$ TW/cm^2, which is sufficient for substantial photoionization and generation of subcritical EHP in FS.[3,30,31] Altogether, small diameter of the luminous channels and gradual increase of their length with pulse energy demonstrate that channels consist of single filaments, since otherwise multimegawatt pulses would produce multiple shorter channels from corresponding multiple filaments.[1]

The above mentioned observations are qualitatively reproducible under different irradiation conditions as well. This point can be illustrated by the optical damage traces in Fig. 3 left by irradiation of FS by femtosecond laser pulses with the central wavelength of 1030 nm (see Sec. II for details). To enhance optical contrast of the damage traces, irradiation by up to $N=100$ pulses per site and tighter focusing by the lens with NA=0.32 were used. The traces coinciding with the luminous channels are awl-shaped and have two characteristic damage zones.[4,29,34,35] In the focus, the damage zone is wider and contains apparent inhomogeneities, whereas behind the focus it becomes narrower and more homogeneous. As known, in the first zone considerable mass transfer occurs resulting in nonhomogeneous modification of the refractive index, while in the second zone the mass transfer is absent and index modification is smooth (optical waveguide recording regime).[1,25,26,29,35–37]

B. Ultrasonic imaging

The recorded ultrasonic transients exhibit strongly asymmetric bipolar pulses with major compression (positive) and accompanying minor rarefaction (negative) phases within the time intervals $t \approx 0.75-1.0$ μs, as illustrated in Figs. 4(a)–4(c), being characteristic of compressive source stress.[38] The subsequent ultrasonic signal at $t > 1$ μs represents acoustic reverberations in the detection system, as shown in Fig. 4(d), exhibiting a transfer function of the transducer to a 10 ns wide purely compressive ablative ultrasonic pulse produced in the near-field by a laser pulse of the same width. For the ultrasonic transducer centered above the filamentary channel as in Fig. 1, the initial delay time of 0.75 μs represents transit from the ultrasonic source to the top surface of the sample $r_{\mathrm{FS}} \approx 3.2$ mm with the longitudinal sound speed $C_{\mathrm{FS}} \approx 5.9$ km/s,[39] and transit across the layer of the lubricating vacuum grease with the thickness $r_{\mathrm{gr}} \approx 0.3$ mm, with the longitudinal sound speed $C_{\mathrm{gr}} \approx 1.4$ km/s (Ref. 39) (the total shortest path between the source and detector $r_{\mathrm{sd}} = r_{\mathrm{FS}} + r_{\mathrm{gr}} \approx 3.5$ mm), thus unambiguously relating the ultrasonic source to the channels. The delay also includes the response time of electronic data acquisition system, which according to our estimates, is shorter than 50 ns.

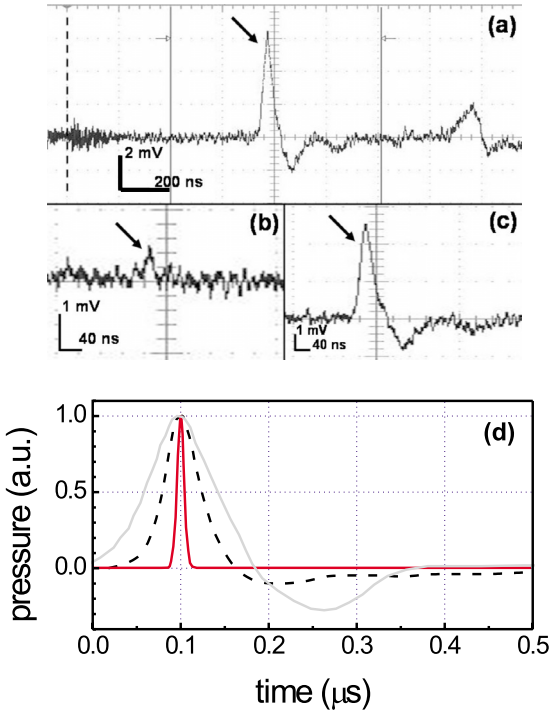

FIG. 4. (Color online) Ultrasonic transients measured after excitation of FS by 800 nm laser pulses having the energy of 65 (a), 10 (b), and 45 (c) μJ. Transfer function of the ultrasonic transducer with the preamplifier (d) represented by its response (dashed line) to a 10 ns wide compressive pulse (solid line). For comparison, theoretical pulse shape of a cylindrical ultrasonic pressure wave adapted from the literature (Ref. 38) is also shown (solid gray line). In (a)–(c), positive and negative pulses signify compression and rarefaction phases of the transients, respectively. In (a), the $t=0$ instant is marked by the vertical dashed line. In (a)–(c), positions of the major compressive pulses are emphasized by arrows, and calibration for vertical and horizontal axes is given by scale bars.

The ultrasonic pulses exhibit continuous asymmetric broadening with a full width in the range of $\tau_{\mathrm{broad}} = 45-110$ ns ($t=0.75-0.86$ μs at the fixed front position) with the laser pulse energy, indicating simultaneous extension and displacement of the effective region of ultrasonic source from the transducer, similar to those of the luminous channels in Fig. 1. Figure 5 describes the broadening as a function of laser pulse energy. The minimal temporal pulse width of about 40 ns at the threshold pulse energy E_T^{ult}

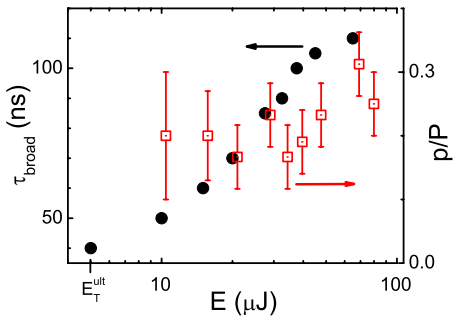

FIG. 5. (Color online) Dependencies of the full width of compression pulses τ_{broad} (full circles) and the ratio of rarefaction pressure p to compression pressure P (hollow squares) on the laser pulse energy E. $E_T^{ult} \approx 5$ μJ indicates the threshold energy for ultrasonic emission at which τ_{broad} is close to ≈40 ns (see the main text).

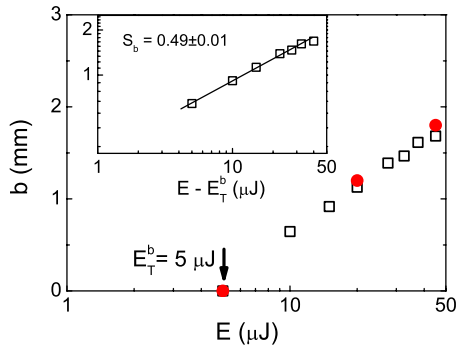

FIG. 6. (Color online) Energy dependence of the channel length as measured from optical images in Fig. 1 (filled circles) and calculated from full widths τ_{broad} of the compression pressure pulses (open squares) with the threshold E_T^b. Inset: energy dependence of the calculated channels length in log-log scale and its linear fit with the slope S_b.

$=5$ μJ is determined by the detector bandwidth[15] rather than properties of our ultrasonic source. Note, that our large-aperture transducer is sensitive to small spatial modifications of the ultrasonic source, since effective aperture of the transducer is smaller than its geometric size due to the radial dependence of the sensitivity.

Also, as is evident from Fig. 5, the ratio between amplitudes of the rarefaction signal, p, and the compression signal, P, remains nearly constant over the broad range of pulse energies, indicating the ultrasonic generation process faster[38] than the ultrasonic transit time over the filament width $2a_{fil}/C_{FS} \sim 10$ μm/6 km/s ~ 1 ns.

Regarding the physical origin of the rarefaction signal, contributions from several processes can be expected. The first of them may come from the instrumental response function of the transducer, which was shown earlier in Fig. 4(d), and features a negative overshoot with amplitude of about 10%. Second, the negative contribution may come from diffraction of a compressive wave, and finally, it may represent a genuine rarefaction component of the pressure created by the source.[38] The two latter effects can be distinguished by analyzing the data acquired during optical observation of the damage traces, described in Sec. III A. Such analysis is based on the spatial coincidence between the ultrasonic source and luminous filamentary channels, whose diameter and length of $a_{fil} \sim 10^{-2}$ mm and $b \sim 1$ mm, respectively, were estimated earlier. Characteristic wavelength of the ultrasonic pulse can be estimated as $\lambda_{ult} = C_{FS}\tau^* \sim 10^{-3}$ mm, where $\tau^* \sim 10^{-9}$ s is the maximum temporal width of ultrasonic pulses excited by femtosecond optical pulses in bulk materials.[40] The measured pulses shown in Fig. 4 are broader because of the limited bandwidth of the transducer. Therefore, the ultrasonic wave propagating away from the source in the far field has cylindrical wave front with curvature radius r, which satisfies the relation $\lambda_{ult}, a_{fil} < r \ll r_{sd}$ and wavefront width l defined as $b \ll l \approx r$. Then, the far field ultrasonic pressure $P(E,r)$ can be expressed in the form adapted from the literature,[23]

$$P(E,r) = P_0(E)\sqrt{\frac{a_{fil}(E)b(E)}{2rl}} \approx P_0(E)\frac{\sqrt{a_{fil}(E)b(E)}}{\sqrt{2}r}, \quad (1)$$

where $P_0(E)$ is the energy-dependent amplitude of the source pressure and $a_{fil}(E)$ and $b(E)$ are energy-dependent diameter and length of the source. It is important to note, that ultrasonic transients acquired in the far field can be obtained from the above expression by accounting for the far-field diffraction effect in the form of characteristic asymmetric bipolar waves for the compressive source stress P_0.[23,38] In our case, however, the large-aperture transducer integrates curved fronts of the transients, thus restoring the initial waveform of the source pressure.[24] Therefore, the presence of extra minor [besides that coming from the transfer function, see Fig. 4(d)] residual rarefaction contribution ≈0.1 P in Fig. 5 indicates that the source pressure is almost purely compressive. The unipolar compressive stress identified above can be associated with generation of electron-ion plasma,[14] electron-phonon (acoustic deformation-potential) interactions,[18,19] thermoelastic effect,[21] or formation of point defects[41,42] resulting in formation of transient or permanent positive strains in fused silica, and thus leading to purely compressive ultrasonic transients. Nevertheless, below we provide some enlightening evidences of its plasma origin, revealed by the source pressure dependence on energy $P_0(E)$.

By ascribing energy-dependent broadening of ultrasonic pulses seen in Figs. 4 and 5 to the upstream elongation of the ultrasonic sources/luminous channels (while their end point coordinate is nearly independent of energy) illustrated in Fig. 1, one can determine the effective length b of the ultrasonic source (channel) from simple geometric arguments. By neglecting the minor displacement of the entire channel with the laser pulse energy in comparison to the shortest ultrasonic path length between the source and detector, r_{sd}, the source length can be expressed by applying the Pythagorean theorem as follows:

$$b(E) \approx \sqrt{\{r_{sd} + C_{FS}[\tau_{broad}(E) - 40 \text{ ns}]\}^2 - r_{sd}^2}. \quad (2)$$

The resulting $b(E)$ dependence shown in Fig. 6 is in good agreement with the optically measured channel lengths in Fig. 2 and has the same threshold energy of $E_T^b = 5 \pm 1$ μJ $\approx E_{opt}$, thus again supporting our identification of the luminous channels as the corresponding ultrasonic sources. This dependence can be approximated well by a square root law of the form $b(E) = b_0\sqrt{E - E_T^b}$ with a constant factor $b_0 \approx 0.28$ mm/μJ$^{1/2}$, or by a linear dependence with a slope parameter $S_b = 0.49 \pm 0.01$ in log-log coordinates (Fig. 6, in-

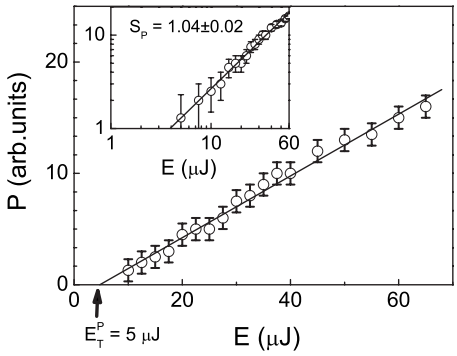

FIG. 7. Energy dependence of the ultrasonic compressive pressure $P(E)$ with the threshold E_T^P. Inset: the same dependence in log-log coordinates and its linear fit with slope $S_P \approx 1$.

set). The constant b_0 expresses dissipative losses due to energy deposition in the dielectric within the laser filaments, supposing that regions of laser beam surrounding the filament serve as an energy reservoir.

Once the functional form of the $b(E)$ dependence is known, one can use the experimental dependence $P(E,r)$ and Eq. (1) to determine the source pressure dependence $P_0(E)$, which describes deposition of the laser pulse energy in the luminous channels. The $P(E)$ dependence at the fixed distance $r_{sd} \approx 3.5$ mm (Fig. 7) is linear and shows the ultrasonic emission threshold $E_T^P = 5 \pm 1$ μJ in good agreement with the previously found values of E_{opt} and E_T^b, also confirming the close physical relationship between the luminous channels and ultrasonic sources. On a logarithmic scale, the dependence has a slope of $S_P = 1.04 \pm 0.02$ (see inset to Fig. 7). Assuming energy-independent diameter of the ultrasonic source (or filament) a_{fil}, the corresponding sublinear source pressure scaling $\propto E^{0.79 \pm 0.03}$ can be obtained from Eq. (1), taking the exponent of 0.79 equal to the difference $S_P - S_b/2$. This value is close to that found in subcritical electron-ion plasmas,[43] which exhibit $\propto E^{0.75}$ law. Taking into account two-dimensional character of transient EHP in the luminous channels[43] yields even closer matching $\propto E^{0.78}$. Good correspondence between the pressure dependencies observed in transient electron-hole plasma in a solid dielectric and in gas-phase electron-ion plasma may look surprising at a first glance. However, it is well-known that in SiO_2 the hole effective mass is large, and these particles are almost localized at atomic cores,[44] thus resembling heavy gas-phase ions in electron-hole collisions. Finally, the similarity between the scaling relationships for electron-ion plasma[43] and for $P_0(E)$ found in this work supports our earlier assumption that filaments occurring in the emission intensity plateau regions have $a_{fil}(E) = a_{fil}$ and the peak laser intensity in the filaments varies as $I \propto E$.

C. Discussion

Results described in Sec. III B demonstrate that femtosecond laser pulses with supercritical powers propagating in FS collapse due to self-focusing and generate light filaments as well as white-light SC emission. Simultaneously, awl-shaped luminous channels filled with subcritical EHP and/or luminescent point defects are formed. Besides these transient effects, permanent optical damage is seen in the corresponding regions of FS.

The conclusion in Sec. III B about the presence of subcritical EHP within the channels (from the $P_0 \propto E^{3/4}$ scaling) is consistent with the sublinear scaling of their emission intensity versus the laser pulse energy as $\propto E^{1/4}$, seen in Fig. 2, since subcritical plasmas have the similar density dependence.[43] The subcritical character of EHP in the filamentary channels is also supported by estimates of the plasma density $N_e \sim 10^{20}$ cm^{-3} for our experiments, while the critical plasma density at the 800 nm wavelength is $N_{crit} \approx 1.8 \times 10^{21}$ cm^{-3}. This is an upper bound estimate based on the energy balance[1] and an assumption of homogeneous dissipation of the entire pulse in the plasma channel,

$$E \sim \Delta_{bg} N_e (a_{fil}^2 b), \tag{3}$$

where $\Delta_{bg} \approx 9$ eV is the direct bandgap in FS,[17] and dimensions of the filament are $a_{fil} \sim 10^{-2}$ mm and $b \sim 1$ mm.

According to Eq. (3), an upper bound estimate of energy density deposited under our experimental conditions ($E \sim 10^{-5}$ J), $\varepsilon \sim E/(a_{fil}^2 b) \sim \Delta_{bg} N_e \sim 10^2$ J/cm^3 is surprisingly low for melting and ablative modification. In FS these processes are known to occur above the threshold energy density[39] of $\varepsilon_{melt,abl} \sim 10^3 - 10^4$ J/cm^3. This indicates that other, "softer" modification mechanisms, e.g., those involving photogeneration of point defects in the filamentary channels and their microscale transport or separation[41] may occur under our experimental conditions, requiring multishot laser exposure and producing the distinct optical damage zones[36,37] seen in Fig. 3. Subcritical plasma is favorable environment for point defect generation due to relatively high thermal energy, $k_B T_e > 1$ eV, of free hot carriers and strongly T_e-dependent carrier self-trapping time.[45] In our case, thermal energy of free hot carriers of $k_B T_e \sim 10$ eV can be directly deduced. This estimate is based on the fact that plasma contribution, $P_{pl} \sim N_e k_B T_e \propto I^{3/4}$ to the source pressure P_0 is dominant, as compared to the response due to electronically driven acoustic deformation potential interaction,[18,22,45] $P_{el} \sim D_{ac} N_e(I) \propto I^{1/4}$, corresponding to $k_B T_e \gg D_{ac}$ for the acoustic deformation potential $D_{ac} \approx 2$ eV in FS.[46] Another estimate of the same order of magnitude for $k_B T_e$ can be also obtained from the modified energy balance Eq. (3) for single laser pulse. This equation is given below together with the scaling of the constituent quantities with laser pulse energy (intensity),

$$\begin{aligned} &E \approx a_{fil}^2 b(E) N(E) [\Delta_{bg} + k_B T_e(E)], \\ &b \propto E^{1/2}, \\ &N_e \propto I^{1/4}, \\ &k_B T_e \propto I^{1/2}, \\ &I \propto E. \end{aligned} \tag{4}$$

Comparing to Eq. (3), the expression for E in Eq. (4) now accounts for the thermal energy of carriers, $k_B T_e$, and energy (intensity) dependencies of b, N_e, and $k_B T_e$. Then, to hold the

same power for E (or I) on both sides of Eq. (4), the expression $[\Delta_{bg}+k_BT_e(E)]$ should scale as[43] $\propto E^{1/4}$ for $k_BT_e \propto I^{1/2}$, which is satisfied only when one has nearly constant ratio $k_BT_e/\Delta_{bg} \approx 1$, i.e., $k_BT_e \approx 9-10$ eV for $\Delta_{bg} \approx 9$ eV in FS.[17] Importantly, such carrier thermal energies are insufficient for the onset of electron avalanche, since in order to obey the momentum and energy conservation laws, energy of the order of $k_BT_e \geq 4\Delta_{bg}$ would be required. This requirement arises due to the high effective mass of heavy holes in FS $m_h^*=(5-10)m_0$, compared to the low effective mass of electrons $m_e^*=(0.3-0.5)m_0$.[44]

The estimated value of k_BT_e is comparable to the corresponding electron quiver energy of $E_q=e^2\lambda^2 I/(2\pi m_e^* c^3) \sim 1-10$ eV (Ref. 47) for $I \sim I_{opt}^{NL} \sim 10-10^2$ TW/cm^2 in the filamentary channels, although typically k_BT_e may increase further above E_q by the factor of $m_h^*/m_e^* \sim 10$ due to multiple consequent electron-hole collisions.[47] Therefore, lower than expected thermal energy of the carriers may be an indication that, besides the impact ionization, another channel of inelastic electron-lattice interactions exists in warm subcritical plasmas. This channel is most likely related to self-trapping of hot carriers and generation of point defects. It is very efficient at the moderate k_BT_e values[45] (estimate of self-trapping rate will be given later) and inhibits carrier heating and subsequent electron avalanche in strong laser field,[48] at least until considerable local disintegration of atomic network and associated optical microscopic damage occurs in the irradiated region. In our case, scaling relationship, $N_e \propto I^{1/4}$, and moderate carrier thermal energy, $k_BT_e \sim 10$ eV, suggest that the dominant ionization mechanism in the warm subcritical plasma is still the impact ionization of the material. This mechanism dominates multiphoton ionization via relatively rare ionizing collisions between a minor fraction of hot carriers and lattice atoms.

The experimentally obtained intensity scaling of the bluish luminescence with the laser pulse energy, $\propto E^{1/4}$, indicates that luminescence intensity may be strongly related to the electron density N_e in the generated EHP, which exhibits similar scaling.[43] Then, in our opinion, there are two possible explanations of the luminescence yield. First, the observed bluish luminescence may result from point defects (with the strongest and medium emission peaks in FS at 280, 400, and 470 nm[25–28]), whose density is linearly proportional to N_e. Second, the luminescence represents visible part of Bremsstrahlung emission from warm EHP with density scaling as $\propto E^{1/4}$ and $k_BT_e \approx 10$ eV nearly constant in the broad range of laser pulse energies of 5–70 μJ. Such plasma provides emission with a spectral peak near the 30 nm wavelength (i.e., in the extreme UV where FS is strongly absorbing[17]) and a slowly varying broadband emission at visible wavelengths (where FS is transparent), consistent with the dominant bluish-white color of the observed luminescence. We believe that such Bremsstrahlung plasma emission is the most plausible source of the observed bluish luminescence, but further static or even time-resolved spectroscopic studies are necessary for its unambiguous experimental identification.

The scaling law $P_0(E) \propto E^{3/4}$ found in our analysis may indicate that laser energy deposition due to the warm subcritical EHP absorption via inverse Bremsstrahlung effect predominates multiphoton absorption (MPA). Hence, in FS the inelastic (self-trapping) electron-lattice collision rate, Γ_{col}, strongly exceeds the MPA rate, $\Gamma_{MPA} \sim N_e/(\tau_p N_{at}) \sim 10^{11}$ s^{-1}, required in order to produce EHP density $N_e \sim 10^{20}$ cm^{-3} during a laser pulse with temporal length of $\tau_p \approx 100$ fs in solids with atomic density $N_a \sim 10^{22}$ cm^{-3}. According to the literature,[3,31,49,50] $\Gamma_{col} \sim 10^{12}-10^{13}$ s^{-1}, which is in good agreement with characteristic subpicosecond times for emission of long-wavelength optical phonons by warm carriers in polar lattices[45] (the latter process resembles self-trapping of hot carriers in FS). It is important to note, that absorption coefficient of warm dense subcritical EHP, as estimated using Drude approximation for the carrier density $N_e \sim 10^{20}$ cm^{-3} and the damping rate $\Gamma_{col} \sim 10^{12}-10^{13}$ s^{-1}, is of the order of 10^3-10^4 cm^{-1}, which by far exceeds the value of ~ 10 cm^{-1} for energy dissipation in the filamentary channels, demonstrating strongly absorbing plasma core of the channels. Therefore, in this fact one may find agreement with the widely accepted concept of "filamentary core and surrounding energy reservoir" structure of laser filaments.[1,2,51] According to this concept, the energy needed for photoionization of atoms in the core of the filament is supplied radially from peripherial regions of the laser beam having lower intensity and lower dissipative losses toward the core. This transfer enables SC generation in the reservoir at much higher pulse energies even in the presence of the opaque EHP plasma in the channel core. Moreover, it appears that self-focusing of the multimegawatt pulses in the channel cores within FS is not compensated by the defocusing EHP effect, but the most intense inner part of the self-focused laser radiation becomes completely utilized for the generation and heating of EHP in the channel core.[52]

Another important result following from the relationship $N_e \propto I^{1/4}$ (where $I \propto E$) found for the filaments/plasma channels is the absence of clamping of the pulse laser intensity I and EHP density N_e. Such clamping was observed in gases and was assumed to be present in solids as well.[1] In contrast, in our case the peak pulse intensity linearly increases as a function of pulse energy E, although the EHP and defect densities (or their emission intensities) vary very slowly $\propto E^{1/4}$. Nevertheless, spatially nonaveraged luminescence intensity profiles shown in Fig. 2(a) show that rather homogeneous energy deposition is provided within the filamentary channel cores for different incident laser energies via energy inflow from the reservoir. This finding is in agreement with permanent damage structures seen in Fig. 3 for $N=100$ showing rather isomorphic features of quite uniform width in the first damage zones (awl heads). Overall, such situation with no clamping may be typical for solid dielectrics where absorbing dense subcritical plasma with the slowly varying density $N_e \propto I^{1/4}$ is readily achievable. For comparison, in normal or compressed gases filament intensity clamping to a fixed value is well established.[1]

In addition to being consistent with main observations of earlier studies conducted in FS and other dielectrics under similar experimental conditions,[1,5–7] our findings are in good qualitative agreement with the results of experiments and theoretical simulations for laser pulses in FS, focused much

more tightly using NA=0.5 optics.[29] The latter work is the most systematic study addressing propagation of femtosecond laser pulses with supercritical power in FS, which is known to us, and available for the comparison despite the big differences in focusing conditions, spatial scales of energy deposition, and incident laser pulse energies. According to Fig. 6, such differences can be reasonably accounted for by using scaling relationship between the length of the laser excitation region and the incident pulse energy. Moreover, in this regime, asymmetric damped, micrometer-long axial pulse intensity profiles, similar to the damped emission intensity profiles in Fig. 2, were predicted and observed.[29] Also, the present study and earlier reports[29] have demonstrated EHP density of similar order of magnitude, $N_e \sim 10^{20}$ cm^{-3}, in the filamentary channels in FS, corresponding to the intensity range of about 30–60 TW/cm^2.[3,31] This finding is also in good agreement with theoretical predictions.[29] Although unlike these theoretical simulations, our study shows rather flat nonaveraged axial intensity profiles in Fig. 2, which are directly related to corresponding axial EHP profiles in the filaments, such comparison may be irrelevant due to unknown internal structure of the millimeter-long filaments (e.g., continuous or discrete multifocii filaments) in this study.

IV. CONCLUSIONS

Summarizing this work, the spatially resolved optical and ultrasonic imaging experiments have revealed self-focusing and filamentation of femtosecond laser pulses having multimegawatt supercritical powers and loosely focused in bulk FS. This conclusion is drawn from the optical observation of millimeter-long awl-shaped luminous channels consisting of warm electron-hole plasma and photogenerated point defects. With increasing laser pulse energy, the channels appear at energy above a certain threshold value and elongate upstream the laser beam, together with upstream movement of nonlinear focus. At even higher pulse energies, forward-propagating SC emission is observed. Ultrasonic imaging of the filaments reveals that with increasing laser pulse energy major compressive ultrasonic pulses appear above the same threshold as needed for the channel observation, and exhibit linearly increasing amplitude as well as significant temporal broadening, indicating the square root energy dependence of the filament/plasma channel length. From these observations, sublinear energy dependence of the source pressure in the channels, which is universal and characteristic feature of subcritical electron-ion plasma, is retrieved.

Altogether, these experimental findings demonstrate formation of subcritical electron-hole plasma channels, followed by point defect generation and permanent optical damage within the channels. Peak intensity of the propagating laser pulses is not clamped, but varies linearly versus the incident pulse energy. Nevertheless, electron-hole plasma density distribution in the filamentary channel cores remains quite homogeneous. The predominant ionization mechanism in the warm subcritical plasmas is most likely associated with moderate avalanche ionization, while the main mechanism of optical absorption is free-carrier absorption via inverse Bremsstrahlung interaction with the polar lattice, resulting in carrier self-trapping. The reported results may also indicate that filaments produced in solid dielectrics by highly supercritical laser pulses can be downscaled in terms of their length as a function of laser pulse power (energy), at least at low pulse energies.

ACKNOWLEDGMENTS

This work was carried out in the framework of Grant-in-Aid from the Ministry of Education, Science, Sports, and Culture of Japan Grant No. 19360322. V.M. and H.M. acknowledge support from KAKENHI Grant-in-Aid for Scientific Research on Priority Area "Strong Photons-Molecules Coupling Fields" Grant No. 470 from the Ministry of Education, Science, Sports, and Culture of Japan. The authors thank UC VINFIN and Dr. I. Pelivanov and Dr. N. Podymova (International Laser Center, Moscow State University) for technical support and valuable discussions.

[1] A. Couairon and A. Mysyrowicz, Phys. Rep. **441**, 47 (2007).
[2] L. Berge, S. Skupin, R. Nuter, J. Kasparian, and J.-P. Wolf, Rep. Prog. Phys. **70**, 1633 (2007).
[3] S. Mao, F. Quere, S. Guizard, X. Mao, R. Russo, G. Petite, and P. Martin, Appl. Phys. A: Mater. Sci. Process. **79**, 1695 (2004).
[4] Z. Wu, H. Jiang, L. Luo, H. Guo, H. Yang, and Q. Gong, Opt. Lett. **27**, 448 (2002).
[5] S.-H. Cho, H. Kumagai, and K. Midorikawa, Appl. Phys. A: Mater. Sci. Process. **76**, 755 (2003).
[6] A. Babin, A. Kiselev, D. Kulagin, K. Pravdenko, and A. N. Stepanov, JETP Lett. **80**, 298 (2004).
[7] A. Horn, E. Kreutz, and R. Poprawe, Appl. Phys. A: Mater. Sci. Process. **79**, 923 (2004).
[8] M. Sakakura, M. Terazima, Y. Shimotsuma, K. Miura, and K. Hirao, Opt. Express **15**, 5674 (2007).
[9] S. Juodkazis, S. Matsuo, H. Misawa, V. Mizeikis, A. Marcinkevicius, H.-B. Sun, Y. Tokuda, M. Takahashi, T. Yoko, and J. Nishii, Appl. Surf. Sci. **197–198**, 705 (2002).
[10] K. Yamasaki, S. Juodkazis, S. Matsuo, and H. Misawa, Appl. Phys. A: Mater. Sci. Process. **77**, 371 (2003).
[11] S. Juodkazis, H. Misawa, T. Hashimoto, E. G. Gamaly, and B. Luther-Davies, Appl. Phys. Lett. **88**, 201909 (2006).
[12] S. Juodkazis, K. Nishimura, H. Misawa, T. Ebisui, R. Waki, S. Matsuo, and T. Okada, Adv. Mater. (Weinheim, Ger.) **18**, 1361 (2006).
[13] J. Yu, D. Mondelain, J. Kasparian, E. Salmon, S. Geffroy, V. Boutou, C. Favre, and J.-P. Wolf, Appl. Opt. **42**, 7117 (2003).
[14] E. Glezer, C. Schaffer, N. Nishimura, and E. Mazur, Opt. Lett. **22**, 1817 (1997).
[15] S. I. Kudryashov, V. D. Zvorykin, A. A. Ionin, V. Mizeikis, S. Juodkazis, and H. Misawa, Appl. Phys. Lett. **92**, 101916 (2008).
[16] V. Mizeikis, S. Juodkazis, T. Balčiūnas, S. Kudryashov, V. Zvorykin, A. Ionin, and H. Misawa, Appl. Surf. Sci. (in press).
[17] *Handbook of Optical Constants of Solids*, edited by E. D. Palik (Academic, Orlando, 1998).
[18] C. Thomsen, H. Grahn, H. Maris, and J. Tauc, Phys. Rev. B **34**, 4129 (1986).
[19] O. Matsuda, O. Wright, D. Hurley, V. Gusev, and K. Shimizu, Phys. Rev. Lett. **93**, 095501 (2004).
[20] B. Daly, T. Norris, J. Chen, and J. Khurgin, Phys. Rev. B **70**, 214307 (2004).
[21] A. Vogel, J. Noack, G. Hütman, and G. Paltauf, Appl. Phys. B: Lasers Opt. **81**, 1015 (2005).
[22] N. Chigarev, D. Y. Parashchuk, Y. Pan, and V. Gusev, J. Exp. Theor. Phys. **94**, 627 (2002).
[23] V. Gusev and A. Karabutov, *Laser Optoacoustics* (AIP, New York, 1993).
[24] T. Khokhlova, I. Pelivanov, V. Kozhushko, A. Zharinov, V. Solomatin, and A. Karabutov, Appl. Opt. **46**, 262 (2007).
[25] N. Fukata, Y. Yamamoto, K. Murakami, M. Hase, and M. Kitajima, Appl. Phys. A: Mater. Sci. Process. **79**, 1425 (2004).

[26]A. Zoubir, C. Rivero, R. Grodsky, K. Richardson, M. Richardson, T. Cardinal, and M. Couzi, Phys. Rev. B **73**, 224117 (2006).
[27]M. Watanabe, S. Juodkazis, H.-B. Sun, S. Matsuo, and H. Misawa, Phys. Rev. B **60**, 9959 (1999).
[28]W. Reichman, D. Krol, L. Shah, F. Yoshino, A. Arai, S. Eaton, and P. Herman, J. Appl. Phys. **99**, 123112 (2006).
[29]A. Couairon, L. Sudrie, M. Franco, B. Prade, and A. Mysyrowicz, Phys. Rev. B **71**, 125435 (2005).
[30]M. Li, S. Menon, J. Nibarger, and G. Gibson, Phys. Rev. Lett. **82**, 2394 (1999).
[31]V. Temnov, K. Sokolowski-Tinten, P. Zhou, A. El-Khamhawy, and D. von der Linde, Phys. Rev. Lett. **97**, 237403 (2006).
[32]N. Nguen, A. Saliminia, W. Liu, S. Chin, and R. Vallee, Opt. Lett. **28**, 1591 (2003).
[33]J. Ashcom, R. Gattas, C. Schaffer, and E. Mazur, J. Opt. Soc. Am. B **23**, 2317 (2006).
[34]C. Schaffer, A. Jamison, and E. Mazur, Appl. Phys. Lett. **84**, 1441 (2004).
[35]S. I. Kudryashov, G. Mourou, A. Joglekar, J. F. Herbstman, and A. Hunt, Appl. Phys. Lett. **91**, 141111 (2007).
[36]J. Chan, T. Huser, S. Risbud, and D. Krol, Appl. Phys. A: Mater. Sci. Process. **76**, 367 (2003).
[37]H. Zhang, S. Eaton, and P. Herman, Opt. Express **14**, 4826 (2006).
[38]C.-Y. Kuo, M. M. F. Vieira, and C. K. N. Patel, J. Appl. Phys. **55**, 3333 (1984).
[39]I. Grigor'ev and E. Meilikhova, *Fizicheskie Velichini* (Energoatomizdat, Moscow, 1991).
[40]H. Hebert, F. Vidal, F. Martin, J.-C. Kieffer, A. Nadeau, T. Johnston, A. Blouin, A. Moreau, and J.-P. Monchalin, J. Appl. Phys. **98**, 033104 (2005).
[41]S. Kudryashov, Proc. SPIE **5647**, 513 (2005).
[42]W. Hayes and A. Stoneham, *Defects and Defect Processes in Nonmetallic Solids* (Dover, New York, 2004).
[43]C. Phipps, T. Turner, R. Harrison, G. York, W. Osborne, G. Anderson, X. Corlis, L. Haynes, H. Steele, and K. Spicochi, J. Appl. Phys. **64**, 1083 (1988).
[44]J. Chelikowsky and M. Schlutter, Phys. Rev. B **15**, 4020 (1977).
[45]P. Yu and M. Cardona, *Fundamentals of Semiconductors: Physics and Materials Properties* (Springer, Berlin, 2002).
[46]J. Graebner, L. Allen, B. Golding, and A. Kane, Phys. Rev. B **27**, 3697 (1983).
[47]N. Koroteev and I. Shumay, *Physics of High-Power Laser Radiation* (Nauka, Moscow, 1991).
[48]B. Rethfeld, Phys. Rev. B **73**, 035101 (2006).
[49]P. N. Saeta and B. I. Greene, Phys. Rev. Lett. **70**, 3588 (1993).
[50]P. Martin, S. Guizard, P. Daguzan, G. Petite, P. D'Oliveira, P. Meynadier, and M. Perdrix, Phys. Rev. B **55**, 5799 (1997).
[51]A. Dubietis, E. Gaižauskas, G. Tamošauskas, and P. Di Trapani, Phys. Rev. Lett. **92**, 253903 (2004).
[52]D. Faccio, A. Averchi, A. Lotti, P. D. Trapani, A. Couairon, D. Papazoglou, and S. Tzortzakis, Opt. Express **16**, 1565 (2008).